MICROSCOPY

Microscopy, 2018, 1–15
doi: 10.1093/jmicro/dfy134

Article

Image segmentation of activated sludge phase contrast images using phase stretch transform

Raymond Bing Quan Ang[1], Humaira Nisar[1,*], Muhammad Burhan Khan[2], and Chi-Yi Tsai[3]

[1]Department of Electronic Engineering, Faculty of Engineering and Green Technology, Universiti Tunku Abdul Rahman, Jalan Universiti, Bandar Barat, 31900 Kampar, Perak, Malaysia, [2]Department of Electrical Engineering, National University of Computer and Emerging Sciences, Shah Latif Town 75030, National Highway (N-5), Karachi, Pakistan, and [3]Department of Electrical and Computer Engineering, Tamkang University, No. 151, Yingzhuan Road, Tamsui District, New Taipei City 25137, Taiwan R.O.C

[*]To whom correspondence should be addressed. E-mail: humaira@utar.edu.my

Received 21 August 2018; Editorial Decision 29 October 2018; Accepted 1 November 2018

Abstract

Activated sludge (AS) is a biological treatment process that is employed in wastewater treatment plants. Filamentous bacteria in AS plays an important role in the settling ability of the sludge. Proper settling of the sludge is essential for normal functionality of the wastewater plants, where filamentous bulking is always a persistent problem preventing sludge from settling. The performance of AS plants is conventionally monitored by physico-chemical procedures. An alternative way of monitoring the AS in wastewater treatment process is to use image processing and analysis. Good performance of the image segmentation algorithms is important to quantify flocs and filaments in AS. In this article, an algorithm is proposed to perform segmentation of filaments in the phase contrast images using phase stretch transform. Different values of strength (S) and warp (W) are tested to obtain optimum segmentation results and decrease the halo and shade-off artefacts encountered in phase contrast microscopy. The performance of the algorithm is assessed using DICE coefficient, accuracy, false positive rate (FPR), false negative rate (FNR) and Rand index (RI). Sixty-one gold approximations of ground truth images were manually prepared to assess the segmentation results. Thirty-two of them were acquired at 10× magnification and 29 of them were acquired at 20× magnification. The proposed algorithm exhibits better segmentation performance with an average DICE coefficient equal to 52.25%, accuracy 99.74%, FNR 41.8% and FPR 0.14% and RI 99.49%, based on 61 images.

Key words: phase contrast image, image segmentation, phase stretch transform, wastewater treatment, activated sludge, filamentous bacteria

Introduction

Activated sludge (AS) process is frequently used in biological treatment of wastewater discharged from municipal and industrial plants. Proper settling of sludge is essential for normal functionality of the wastewater treatment plants. The efficiency of the AS process is highly influenced by the solid–liquid separation which is affected by the structure and strength of the flocs. Flocs are microbial aggregates present in wastewater along with filamentous bacteria. Settling ability and compaction of the floc particles is associated with the quantity of filamentous bacteria in the AS. Lack of filamentous bacteria results in an abnormal condition of pinpoint flocs [1], whereas overgrowth of filamentous bacteria results in abnormal condition of filamentous bulking. It results in decreased settling ability and compactness of the flocs [2]. Filamentous bulking is a common problem that is present in wastewater treatment plants around the world. Evaluation and modelling of the wastewater treatment by using image processing and analysis offers an alternative way of monitoring AS process. The application of automated image analysis on AS process has been increased in the recent years [3–6].

Phase contrast microscopy (PCM) is widely used in biological and medical research to examine the live organisms and micro-organisms by enhancing the contrast of transparent components in the cell. In order to observe filaments in AS wastewater both bright field and PCM is used [2,3]. However PCM exhibits better discrimination of thin filamentous bacteria as they appear darker in phase contrast images as compared to the background. Hence the filamentous bacteria can be viewed at lower objective magnification without staining in PCM as compared to bright field microscopy where at low magnifications filaments are not easily visible. Observing filaments at low magnifications also results in time saving when acquiring images of the AS samples [7]. The dark colour of the filaments and bright flocs provide a good contrast for segmentation based on the intensity. However, PCM has its own problems. In the phase contrast images, two different types of artefacts known as halos and shade-off are present. Halos appear as bright region around the boundaries of flocs and filaments making segmentation difficult. Whereas shade-off causes decreased contrast between the flocs and the background that results in introduction of foreground noise during segmentation. The shade-off and halo artefact that exists in PCM makes it difficult to identify the boundary of the flocs and filaments.

Kaur and Kaur [8] reported a review of popular segmentation methods such as threshold based methods, edge detection based methods, region based methods, clustering based methods, watershed based methods, partial differential equation based segmentation methods and artificial neural network based segmentation methods. Many authors have proposed algorithms for segmentation of bright field microscopic images of AS. Lee *et al.* [9] preprocessed the bright field image followed by variance based thresholding. Wu and Wheatley [10] used thresholding to binarize the image, followed by morphological opening. Mesquita *et al.* [3] applied background removal and histogram equalization followed by thresholding.For phase contrast images, Khan *et al.* [4] proposed histogram based thresholding using inter-means algorithm. Otsu thresholding, channel based algorithm, Sobel edge based algorithm and Bradley based algorithm were adopted by Nisar *et al.* [11]. They suggested that edge based algorithm is the best for phase contrast images. Khan *et al.* [12] conducted a comprehensive review of nine segmentation algorithms, that includes Saturation based segmentation, edge based segmentation, *K*-means, Watershed based segmentation, Kittler, split and merge method, top-bottom-hat, local adaptive thresholding based segmentation and texture based segmentation. They detected the flocs using Otsu thresholding followed by dilation and reduced radius of gyration (RRG).

Jenné *et al.* [13] used five different shape parameters, i.e. aspect ratio, roundness, form factor, fractal dimension and RRG to discriminate between the flocs and the filaments. They found out that the most suitable parameter used to differentiate between flocs and filaments is RRG while the most unsuitable parameter is form factor. RRG has been widely used by many authors to filter out small debris and determine the true filaments [3,4,9,14].

Many researchers [15–17] have used phase stretch transform (PST) to enhance digital images. PST can be applied to both digital images as well as time series data and has been used for edge detection in biomedical images [16,18]. PST has also been applied in super-resolution localization microscopy for enhancing the resolution when imaging a single molecule [19]. The algorithm has been open sourced on GitHub and Matlab Central File Exchange [20]. PST applies a 2D phase function to the image in the frequency domain. The amount of phase applied to the image depends on the frequency. It is known that the edges of an image contain high frequency components, hence PST emphasizes the edges by giving more importance to the higher frequency features present in the edges. Finally, the edges can be extracted by thresholding the PST output phase image [16]. This method is found to be very useful by many researches [15–20] and gives promising results.

Hence in this paper we have used PST proposed by Asghari and Jalali [15,16] for the segmentation of AS filamentous bacteria and evaluated the performance of the developed algorithm using different assessment metrics. In

the following sections we will discuss the proposed method and assessment in detail.

Methods

Image acquisition

Samples from eight municipal wastewater treatment plants and one experimental setup were collected to build the image database. Olympus Microscope BX43 with Olympus CellSens Dimension image acquisition software was used to capture phase contrast images. 12 µL of sample collected from AS wastewater treatment plant was placed on a microscopic slide covered by a $18 \times 18\ mm^2$ cover slip. All images were saved in the TIFF file format with 1224×960 pixels image resolution. The images were acquired at 10× and 20× magnifications. Magnifications lower than 10× were not considered as filaments are not easily visible at lower magnifications whereas magnifications higher than 20× may require many images to cover a single filament, if the filament size is long. Hence, 10× and 20x magnifications were found suitable for the present work. At 10× magnification, the pixel size is 0.7015 µm/pixel and at 20x magnification the pixel size is 0.3481 µm/pixel. From the database, 61 phase contrast images (32 images with 10× magnification and 29 images with 20× magnification) were randomly selected to assess the proposed algorithm.

Image segmentation algorithm

The proposed algorithm consists of two main parts: Identification of flocs and filamentous bacteria as foreground and separation of filamentous bacteria from the foreground. The flow diagram is illustrated in Fig. 1.

Gaussian low pass filter

The RGB image (red, green blue) is converted into the grayscale image. Gaussian low pass filter is applied to the grayscale image to reduce the random noise by blurring the image. The blurring effect depends on the bandwidth of the Gaussian localisation filter (Δf) used. Lower bandwidth will result in better noise reduction but the edge information may be lost after filtering. Bandwidth of 0.25 is selected to reduce the noise in the image while the edges are still preserved and are detectable by the PST.

Phase stretch transform

PST is proposed by Asghari and Jalali [15,16]. It applies a 2-dimensional (2D) phase kernel to the frequency domain image to highlight the edge information. The amount of the phase applied to the image is associated with the frequency. Edges consist of high frequency features, and hence, higher phase will be assigned to them. PST of a 2D image can be given by the following equation [15,16]:

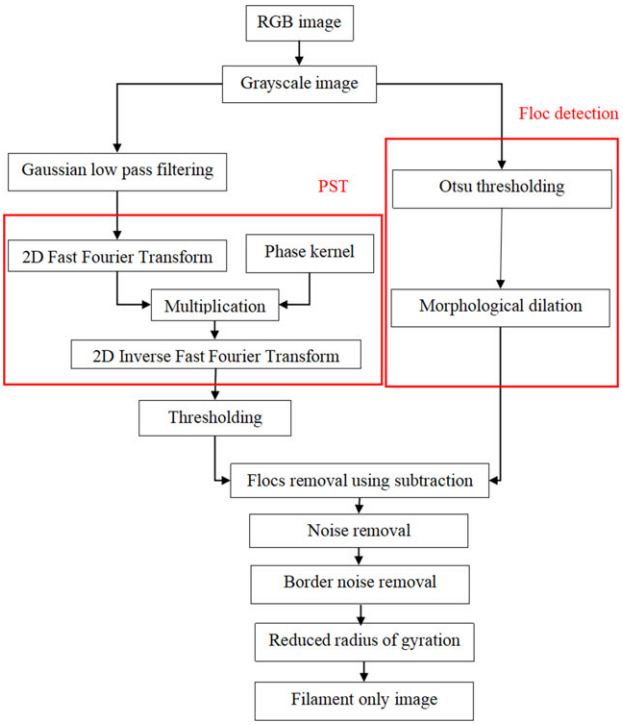

Fig. 1. Flow diagram of proposed segmentation algorithm.

$$A[n, m] = \measuredangle\langle \mathrm{IFFT2}\{\tilde{K}[p, q] \cdot \mathrm{FFT2}\{B[n, m]\}\}\rangle \quad (1)$$

where $B[n, m]$ is the input image, $A[n, m]$ is the output phase image, n and m are 2D spatial variables. $\measuredangle\langle\cdot\rangle$ refers to the angle operator, FFT2 and IFFT2 are the 2D Fast Fourier Transform and the 2D Inverse Fast Fourier Transform, respectively, and $\tilde{K}[p, q]$ is the phase kernel described by the frequency dependent phase function in the following equation:

$$\tilde{K}[p, q] = e^{j\phi[p,q]} \quad (2)$$

For edge detection, the phase derivative $PD[p, q]$ should be a linear or sublinear function with respect to p and q frequency variables. Inverse tangent function as shown in the following equation can be used to create such phase derivative profiles:

$$\phi[p, q] = \phi_{\mathrm{polar}}[r, \theta] = \phi_{\mathrm{polar}}[r] = S\frac{W \cdot r \cdot tan^{-1}(W \cdot r) - \frac{1}{2} \cdot \ln(1 + (W \cdot r)^2)}{W \cdot r_{\max} \cdot tan^{-1}(W \cdot r_{\max}) - \frac{1}{2} \cdot \ln(1 + (W \cdot r_{\max})^2)} \quad (3)$$

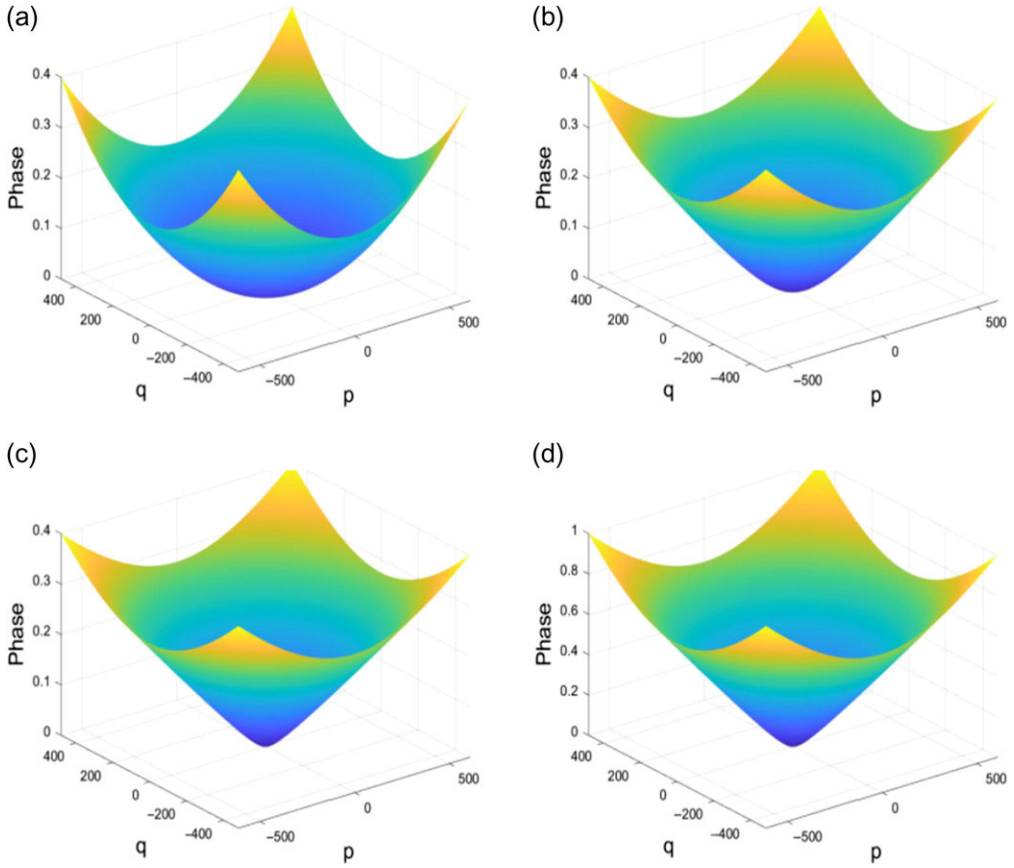

Fig. 2. Comparison of 2D phase kernels. (a) $W = 0.1$, $S = 0.4$, (b) $W = 10$, $S = 0.4$, (c) $W = 40$, $S = 0.4$ and (d) $W = 40$, $S = 1$.

From the equation, $r = \sqrt{p^2 + q^2}$, $\theta = tan^{-1}(\frac{p}{q})$ and r_{max} refers to the maximum value of r. S and W refer to the strength and warp variables used to construct the phase kernel.

The first stage of PST is to convert the image from spatial domain into frequency domain using 2D FFT. Then, the resultant frequency domain image is multiplied by a phase kernel described in Eq. (1). Variables S and W decide phase derivative of the phase kernel and control the amount of phase applied to each frequency. Figure 2 compares four phase kernels constructed using different S and W values. Each of them produce different phase derivative profiles, as shown in Fig. 3.

Referring to Fig. 3, a near zero W value results in linear phase derivative profile. As W increases up to 40, the curvature of the phase derivative profile increases. The phase profile with higher W has almost the same phase derivative when away from the origin. In contrast, the phase derivative will experience significant drop when it is closer to the origin.

The output phase image is obtained by performing 2D IFFT to convert the resultant image from frequency domain to the spatial domain. Figure 4 shows an example of output phase image with different viewpoints. Edges in an image represent high frequency features. The sharp transition edges are assigned high phase values illustrated in yellow and red colours in Fig. 4. The background which has somewhat uniform intensity exhibits low frequency features. Thus, low phase value is assigned to low frequency background shown in cyan colour.

One-level thresholding

In Fig. 4 negative phase values are shown by the blue colour. These negative phase values are removed from further processing. It is observed that the pixels with negative phase values correspond to the pixels with the halo artefacts in the foreground in the original image. Halo artefact appears as bright halos around the borders of flocs and filaments [7]. These halos which surround the flocs and filaments have negative phase values when PST is applied, hence the pixels with negative phase values are considered undesirable and removed from further processing otherwise segmentation accuracy will be affected.

In order to extract the edges from output phase image, it is binarized using one-level thresholding, which only considers positive phase values. The threshold point is fixed at 0.002 empirically, parameters W and S are varied to observe the segmentation results. Figures 5 and 6

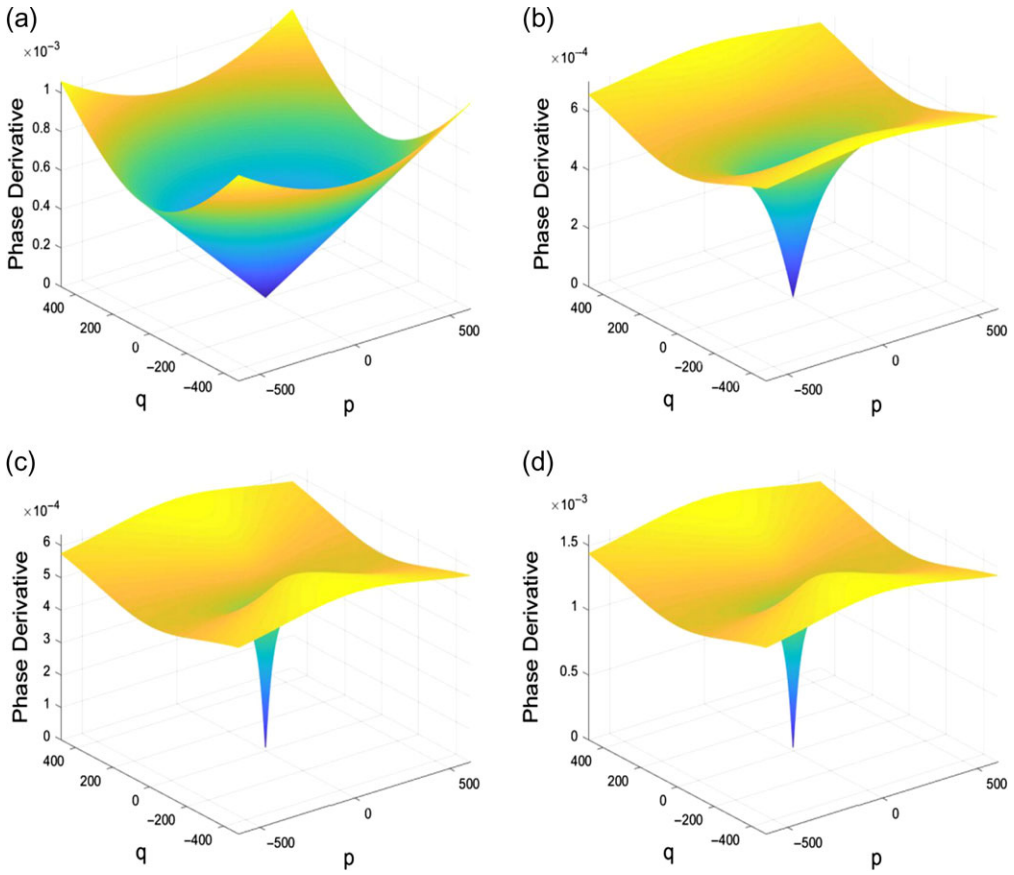

Fig. 3. Comparison of 2D Phase derivative profiles. (a) $W = 0.1$, $S = 0.4$, (b) $W = 10$, $S = 0.4$, (c) $W = 40$, $S = 0.4$ and (d) $W = 40$, $S = 1$.

illustrate the binary image results using different W and S values.

A larger W in phase derivative results in sharper edge but it is prone to noises. In Fig. 5b, only sharp edges with high intensity transition were included; whereas the soft edges failed to be detected, which caused under segmentation. As the value of W increases to 10 as shown in Fig. 5c, only some soft edges were partially detected. When W increases to 40, most of the soft and sharp filaments were preserved successfully but it gives lower noise performance and is more sensitive to the shade-off artefact. It was observed that the value of W equal to 40 gives the best results.

A higher value of S in phase derivative allows the segmentation to preserve all the filaments but it falsely detects large number of isolated pixels as foreground. In Fig. 6a, only sharp edges with high intensity transitions were identified whereas the soft edges were not detected. In addition although filaments are detected, but their pixels are not joined together; hence they will be removed in the subsequent morphological operations and post-processing steps, which will result in under segmentation of filaments. As S increases to 0.4 as shown in Fig. 6b, some soft edges were slightly detected. At the same time, noise was increased. Finally when S increases to 1, all filaments were detected successfully but the segmentation is very sensitive to noise and shade-off as shown in Fig 6c and d. Now it is difficult to remove the connected noise during the post-processing as there are falsely segmented filaments when S is high. In order to deal with these false filaments, more powerful and advanced post-processing steps are required. It is also observed that inspite of W and S been applied, halo artefact is invariant in PST based segmentation. The best segmentation results are obtained with values of $S = 0.4$ and $W = 40$ for the shade-off artefact, and hence will be used throughout the paper for segmentation.

Flocs detection and removal

In AS phase contrast images, the flocs appear brighter than the background and the filaments. Therefore, flocs can be easily segmented from the grayscale image by applying Otsu thresholding [21] method. Otsu thresholding works well with phase contrast images that have bimodal histogram. It calculates the threshold level such that the inter-class variance is maximum. The Otsu threshold level is multiplied by 1.2 so that it's suitable for images with both unimodal and bimodal histograms. After the flocs are detected, morphological dilation is performed to fill in the

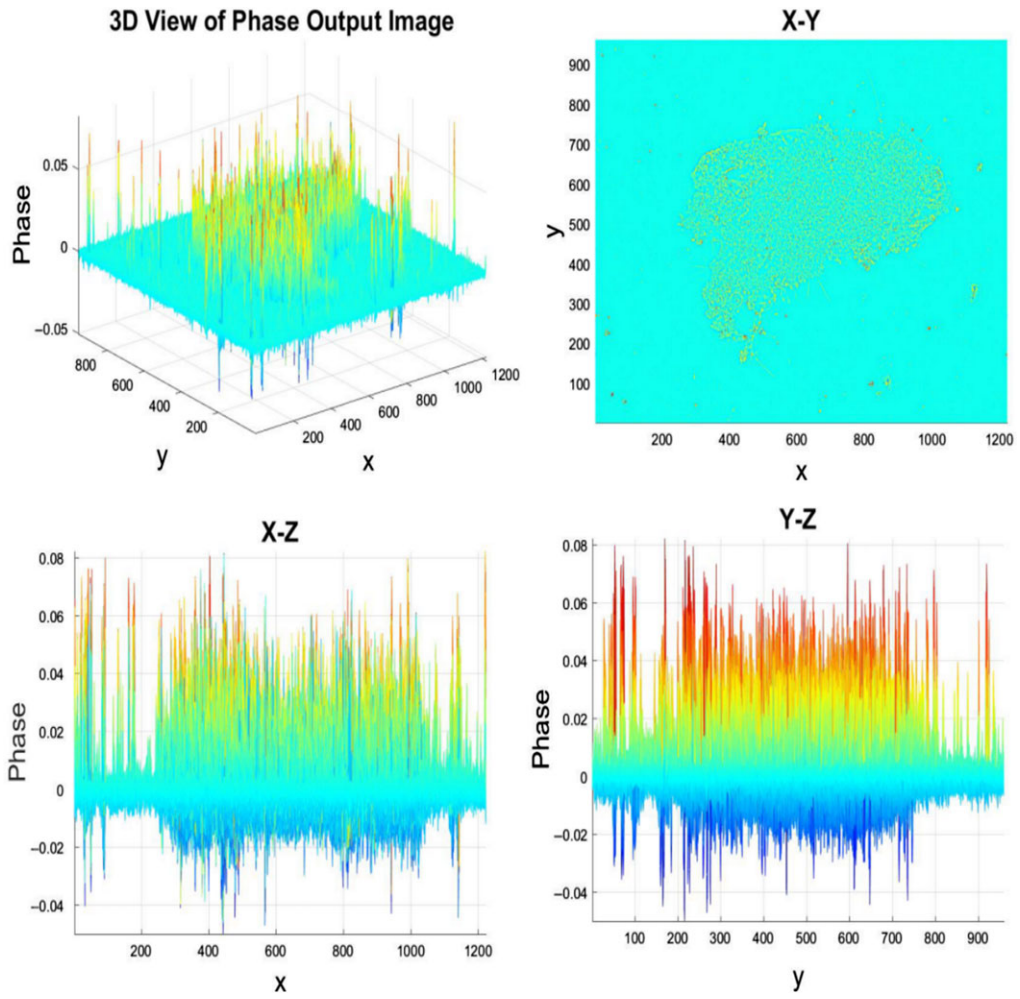

Fig. 4. Output phase image in different viewpoints.

holes and improve the boundary of the flocs. The resultant mask (floc) is subtracted from the segmented binary image obtained using PST, leaving only filaments in the output image. The example of Otsu thresholding of images with unimodal and bimodal histograms is shown in Figs. 7 and 8.

Noise removal

The segmentation of phase contrast images using PST misclassifies some objects as foreground. These falsely detected pixels can be categorised into two types, random noise and noise at the border as shown in Fig. 9. Here two methods are used to remove them while retaining the filament pixels. In the first stage, objects that have pixels less than 20 will be removed using area opening.

An algorithm is developed to eliminate the border noise that cannot be removed by the previous step. This algorithm first defines a frame with a margin of 10 pixels on each side. The defined frame is shown in Fig. 10. Then, connected pixels are labelled to obtain the location of each pixel. If 50% of the pixels in the region are within the margin, it is identified as border noise. Green colour shows the defined margin whereas red pixels represent the detected border noise. Pseudo code of the algorithm is shown below:

```
Label object in the binary image.
Extract x and y coordinate information for each pixel in the object.
    If x ≥ (total column-10) or x ≤ 10
        Pixel is marked
    Else if (y ≥ total row-10) or y ≤ 10
        Pixel is marked
    Else
        Pixel not marked
    End if
If marked pixel is more than 50% of the total pixels of the object
        Remove the object because it's border noise
    Else
        Keep the object because it's filament
```

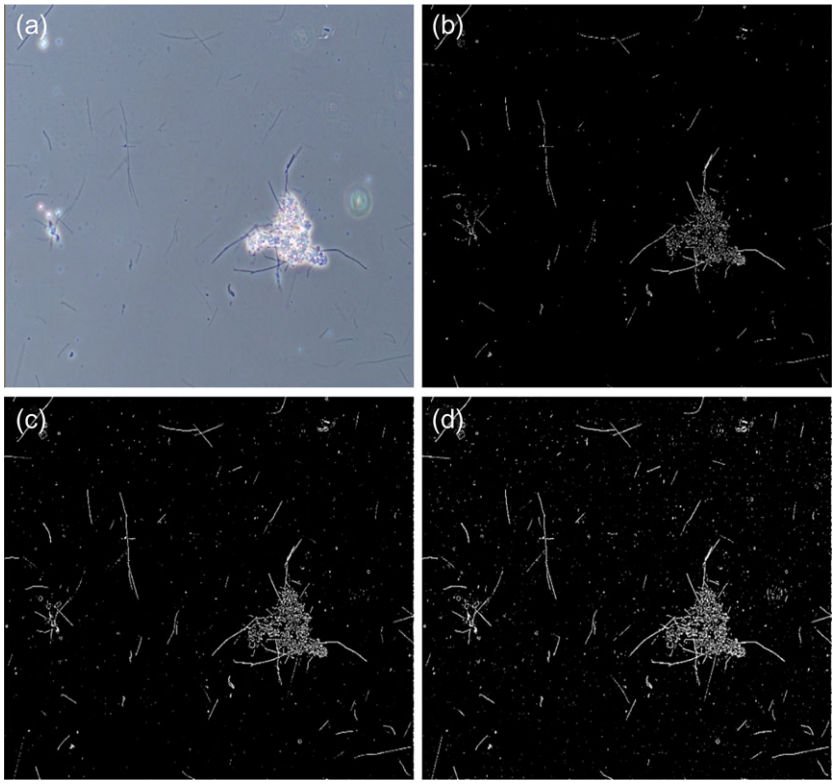

Fig. 5. Effect of Warp (W) on phase contrast image; (a) original image and (b–d) the comparison of threshold image with different W values using strength (S) = 0.4: (b) $W = 1$, (c) $W = 10$ and (d) $W = 40$.

Reduced radius of gyration

RRG is used to distinguish between flocs and filaments (which are normally elongated). This method calculates the radius of gyration of all identified connected components. However it will not work on the filaments that are attached to the flocs. The connected components with radius of gyration less than a defined threshold will be removed while retaining the objects with radius of gyration higher than the threshold. RRG can be defined as follows [14]:

$$\mathrm{RRG} = \frac{\sqrt{M_{2x} + M_{2y}}}{D_{\mathrm{eq}}/2}, \quad D_{\mathrm{eq}} = 2\sqrt{\frac{A}{\pi}}$$
$$M_{2x} = \frac{\sum_{i=1}^{N}(x_i - x_g)^2}{N}, \quad M_{2y} = \frac{\sum_{i=1}^{N}(y_i - y_g)^2}{N}$$
$$x_g = \frac{\sum_{i=1}^{N} x_i}{N}, \quad y_g = \frac{\sum_{i=1}^{N} y_i}{N} \tag{4}$$

where i is the pixel of an object with location (x_i,y_i) and D_{eq} is the diameter of circle with area equivalent to the object's area A. The total amount of object pixels is represented by N. x_g and y_g are the coordinates of the object's centroid. M_{2x} and M_{2y} refer to the momentum in each dimension. The threshold for radius of gyration is set to 1.2 by subjective iteration.

Performance assessment

In order to evaluate the accuracy of the segmentation algorithm, the ground truth images are prepared by manual drawing using GIMP software [22]. True positive (TP), true negative (TN), false positive (FP) and false negative (FN) are determined for performance measurement. TP is defined as the intersection of pixels between the segmented image and the ground truth, showing the pixels that are correctly segmented. Whereas FP pixels are the segmented pixels that do not match with the ground truth. FN pixels are marked in ground truth image but not in the segmented image. Finally, the TN pixels are not marked by the ground truth image nor the segmented image. For performance assessment DICE coefficient, FP rate (FPR), FN rate (FNR) and accuracy are calculated. The formulas are expressed as follows:

$$\mathrm{DICE} = \frac{2|\mathrm{X} \cap \mathrm{Y}|}{|\mathrm{X}| + |\mathrm{Y}|} = 2 * \frac{\mathrm{TP}}{\mathrm{FN} + 2 * \mathrm{TP} + \mathrm{FP}} \tag{5}$$

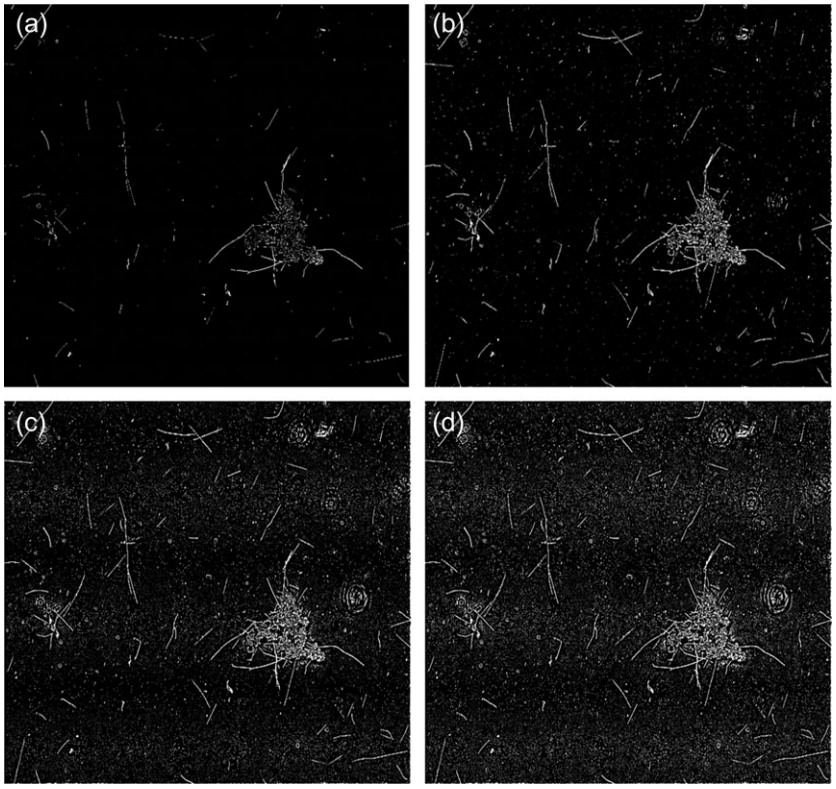

Fig. 6. Effect of strength (S) on the threshold image using different S values using warp (W) = 40: (a) $S = 0.1$, (b) $S = 0.4$, (c) $S = 0.8$ and (d) $S = 1$.

$$\text{FPR} = \text{Fallout} = \frac{\text{FP}}{\text{FP} + \text{TN}} \tag{6}$$

$$\text{FNR} = \text{Miss rate} = \frac{\text{FN}}{\text{FN} + \text{TP}} \tag{7}$$

$$\text{Accuracy} = \frac{\text{TP} + \text{TN}}{\text{TP} + \text{TN} + \text{FP} + \text{FN}} \tag{8}$$

Rand index (RI) suggested by Rand [23] is used to evaluate the performance of clustering methods. It shows the similarity between two data clustering methods. RI is computed as the ratio of similar assignment of pair of pixels in both clusterings divided by total number of pairs. The RI is given by the following equation:

$$\text{RI}(S1, S2) = \frac{\sum_{i<j}^{N} C_{ij}}{\binom{N}{2}} \tag{9}$$

where N is the total number of the pixels in the image, $\binom{N}{2}$ is the total number of combinations of 2 pixels drawn from N pixels and C_{ij} is given in the following equation:

$$C_{ij} = \begin{cases} 1, \textit{pixel pair that are simultaneously identified as either foreground or background in both } S1 \textit{ and } S2 \\ 1, \textit{pixel pair that are simultaneously indentied as neither foreground nor background} \\ 0, \textit{in both } S1 \textit{ and } S2 \textit{ otherwise} \end{cases} \tag{10}$$

Results and discussion

The first step towards the performance assessment of the proposed segmentation method is to identify its apparent failures. The images with subjectively obvious false detections were considered as failed segmentation. Khan *et al.* [12] reported nine different algorithms for segmenting phase contrast images of AS. The algorithms include saturation based [12], edge based (Sobel) [12], K-means [24], watershed algorithm [25], Kittler [26], Split-merge [12], top-bottom hat [27] and two proposed methods [12]. The comparison of the subjective evaluation of these segmentation algorithms and the proposed algorithm based on 61

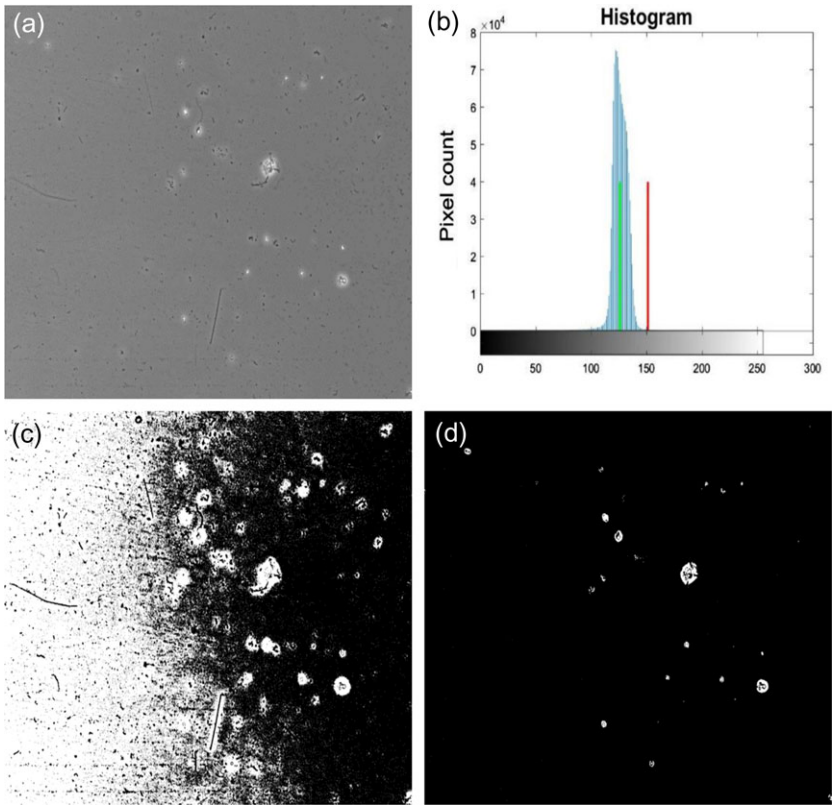

Fig. 7. Otsu thresholding of phase contrast image with unimodal histogram: (a) grayscale image, (b) histogram of grayscale image, (c) segmented image using first vertical line and (d) segmented image using second vertical line.

images is shown in Table 1. Of the 61 phase contrast microscopic images, the proposed method failed to segment the filaments in two images with percentage failure of 3%. The proposed method can be considered as the second best algorithm after Sobel edge detection algorithm based on subjective evaluation.

Next, we performed the objective assessment to evaluate the efficiency of the segmentation algorithms using five parameters including DICE coefficient, accuracy, FNR, FPR and RI. A total of 61 images (31 images of 10× magnification and 29 images of 20× magnification) were selected. The mean and standard deviation of each parameter is tabulated in Tables 2 and 3 respectively. The 20× magnification images performed better with respect to accuracy, FPR and RI, whereas the 10× magnification images have better performance in terms of FNR and DICE coefficient. Small FNR (implies that TP is much greater than FN) results in better segmentation of filaments. In other words, high FNR indicates greater under segmentation of the filaments. Moreover, high DICE coefficient in 10x magnification is caused by lower FN. Conversely, over segmentation of filaments results in increase in FP and FPR, that drops accuracy. From Table 3, we see that 10× magnification images give least variations across DICE coefficient and FNR, but 20× magnification has lower variations in accuracy, RI and FPR. The proposed algorithm is more suitable to perform segmentation under 10× magnification as it gives better performance in terms of DICE coefficient and less FNR variations. Table 4 shows the overall mean and standard deviation values based on the assessment of 61 phase contrast images.

Khan *et al.* [12] removed 17 outlier images and selected 44 images that are apparently successful to assess the segmentations. Therefore, the comparison of mean and standard deviation values of these 44 images was performed. Comparisons of mean and standard deviations for five algorithms are shown in Tables 5 and 6 respectively. The best result is highlighted using red colour, whereas blue colour represents the second best result. The proposed algorithm gives better segmentation performance as compared to the other four algorithms with mean accuracy 0.9977, RI 0.9954, FNR 0.4091 and FPR 0.0013. Comparing with Sobel edge detection shown in blue colour, the accuracy has improved by +0.0007 and RI is increased by +0.0015. The FNR has also improved significantly by −0.2721 compared with Method-II. The proposed algorithm has least under segmentation of filaments.

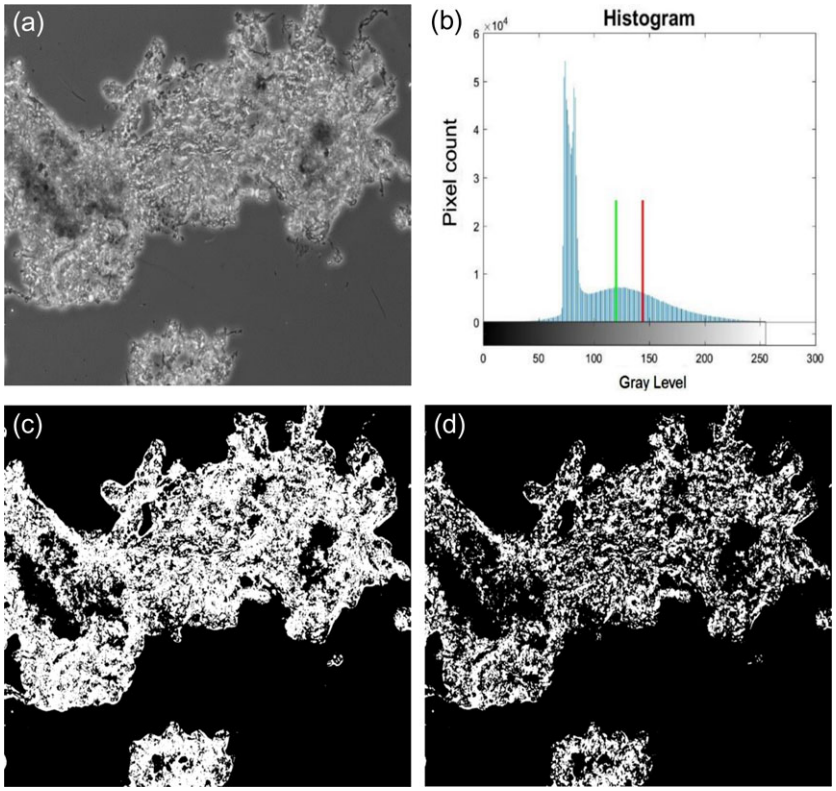

Fig. 8. Otsu thresholding of phase contrast image with bimodal histogram: (a) grayscale image, (b) histogram of grayscale image, (c) segmented image using first vertical line and (d) segmented image using second vertical line.

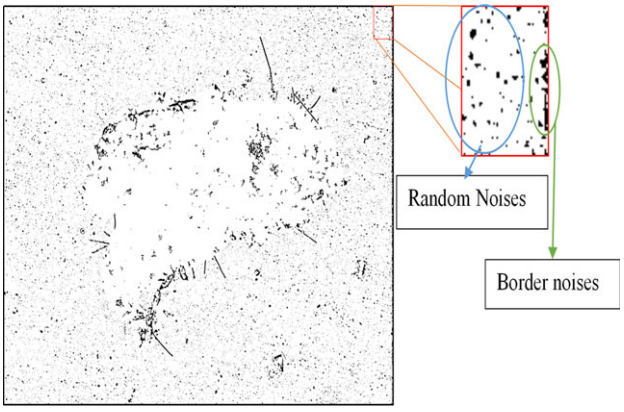

Fig. 9. Illustration of random noise and border noise in complemented image.

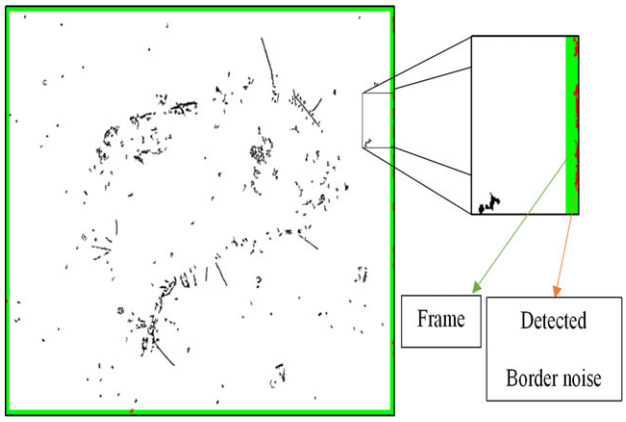

Fig 10. Defined frame and detected border noise in complemented image.

However, it has greater FPR than Sobel edge detection, Method-II, Watershed and Kittler algorithms, which implies that the algorithm tends to over segment the filaments. The proposed algorithm has least variation compared with other four algorithms in terms of accuracy, RI and FPR. However, its FNR variation is greater than Sobel edge detection, Watershed based and Kittler algorithm but smaller than Method-II. Sample images with best and worst FNR results are shown in Figs. 11 and 12, and best and worst FPR results are shown in Figs. 13 and 14 respectively. Performance assessment metrics for Figs 11–14 are given in Table 7.

From Fig. 11, it is observed that the FNR is very small due to small FN compared to TP. It can be clearly observed that the proposed algorithm detects most of the filaments with small over segmentation. Therefore, increase in FP results in high FPR. Sobel-based algorithm under

Table 1. Comparison of failed segmentations

Algorithm	Number of failed segmentations	Percentage failure (%)
Proposed method based on PST	2	3
Saturation [12]	29	48
Edge (Sobel) [12]	1	2
K-means [24]	24	39
Method-I [12]	13	21
Method-II [12]	9	15
Watershed [25]	5	8
Kittler [26]	5	8
Split-merge [12]	33	54
Top-bottom-hat [12]	16	26

Table 2. Mean values of segmentation assessment under different magnifications

Magnification	DICE	Accuracy	FNR	FPR	RI
10×	0.5475	0.9972	0.3336	0.0019	0.9943
20×	0.4950	0.9977	0.5145	0.0009	0.9955

Table 3. Standard deviation of segmentation assessment under different magnifications

Magnification	DICE	Accuracy	FNR	FPR	RI
10×	0.1672	0.0022	0.2003	0.0017	0.0044
20×	0.2362	0.0021	0.2275	0.0012	0.0042

Table 4. Mean and standard deviation values based on 61 images

	DICE	Accuracy	FNR	FPR	RI
Mean	0.5225	0.9974	0.4180	0.0014	0.9949
Standard deviation	0.2030	0.0022	0.2303	0.0015	0.0043

Table 5. Comparison of mean values of segmentation assessment metrics

Algorithm	Accuracy	FNR	FPR	RI
Proposed method based on PST	0.9977	0.4091	0.0013	0.9954
Edge (Sobel) [12]	0.9970	0.8266	0.0006	0.9939
Texture based (Method-II) [12]	0.9887	0.6812	0.0094	0.9794
Watershed [25]	0.9967	0.8868	0.0008	0.9933
Kittler [26]	0.9965	0.946	0.0007	0.9930

segments the filaments more than the proposed algorithm, which results in higher FN and FNR. On the other hand, Fig. 12 shows the worst FNR result among the 61 images. The proposed algorithm under segments the filaments causing low TP. The amount of FN is much greater than TP

Table 6.. Comparison of standard deviation of segmentation assessment metrics

Algorithm	Accuracy	FNR	FPR	RI
Proposed method based on PST	0.0016	0.2343	0.0013	0.0032
Edge (Sobel) [12]	0.0025	0.2196	0.0015	0.0051
Texture based (Method-II) [12]	0.0334	0.2602	0.034	0.0568
Watershed [25]	0.0021	0.1204	0.0014	0.0042
Kittler [26]	0.0029	0.1348	0.002	0.0058

Table 7.. Performance assessment metrics for Figs 11–14

Figure	Algorithm	Accuracy	FNR	FPR	RI
11	Proposed	0.9963	0.0670	0.0033	0.9927
	Sobel [12]	0.9952	0.4045	0.0027	0.9905
12	Proposed	0.9980	0.8885	0.0003	0.9961
	Sobel [12]	0.9980	0.9378	0.0003	0.9960
13	Proposed	0.9977	0.8861	0.0	0.9954
	Sobel [12]	0.9974	1.0	0.0	0.9949
14	Proposed	0.9934	0.0952	0.0061	0.9868
	Sobel [12]	0.9929	0.7986	00.0022	0.9859

results in large FNR. Sobel based algorithm has greater under segmentation of filaments compared with the proposed algorithm, which causes higher FNR. The large amount of TN results in very small FPR even if it is a failed segmentation.

In case of best FPR shown in Fig. 13, it is observed that both algorithms under segment the filaments, causing the high FN and FNR. Since the Sobel based algorithm does not detect any filament, the TP is zero and cause unity FNR. Both algorithms do not over segment the filaments which give zero FP and zero FPR. The accuracies are always high (>0.95) due to large TN. The number of filament pixels are much less as compared to the background. Even for the failed segmentation as shown in Fig. 13d, it can achieve accuracy of 0.9974. Same happens with RI. For the worst FPR which was shown in Fig. 14, it is observed that the proposed algorithm significantly over segments the filaments, high FP providing large FPR. Sobel based algorithm has lower over segmentation of filaments compared with the proposed algorithm, therefore it gives lower FPR. However, Sobel based algorithm has under segmented more filaments when compared with the proposed algorithm, which results in larger FNR. The proposed algorithm has better performance in terms of FNR which has lower probability to under segment the filaments. However, it tends to over segment the filaments.

Conclusion remarks

In this research, filamentous bacteria in phase contrast microscopic images of AS have been successfully

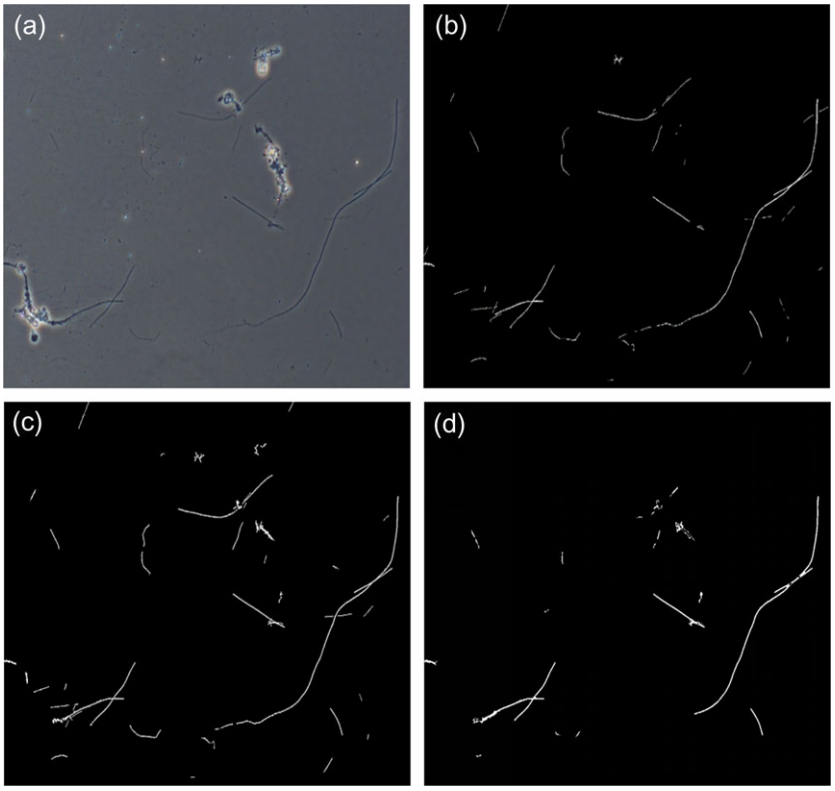

Fig. 11. Image and its segmentation with best FNR: (a) original image, (b) ground truth image, (c) proposed algorithm and (d) Sobel-based algorithm.

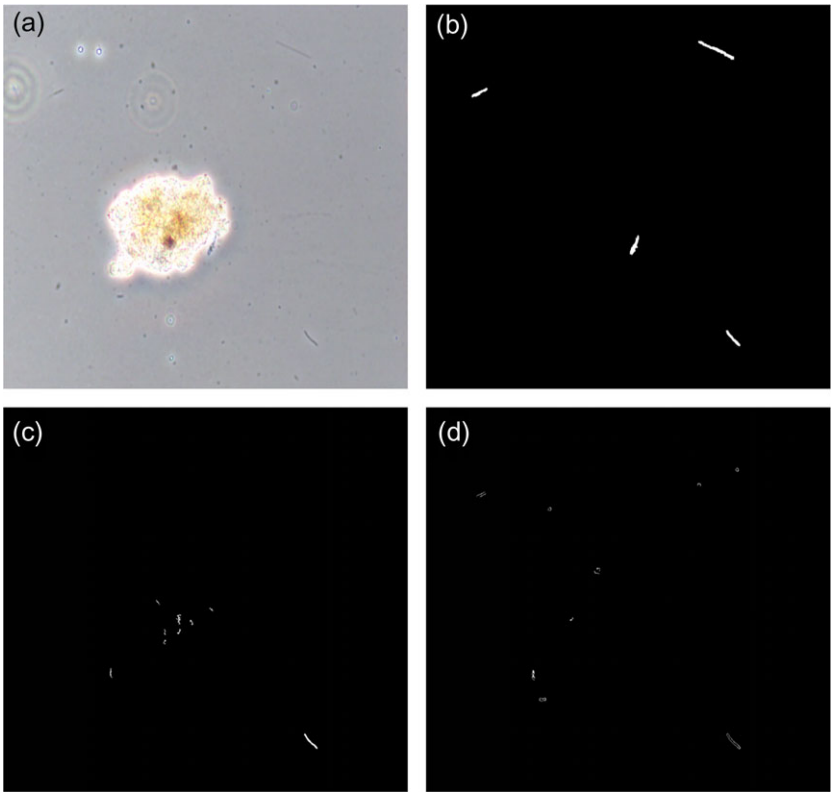

Fig. 12. Image and its segmentation with worst FNR: (a) original image, (b) ground truth image, (c) proposed algorithm and (d) Sobel-based algorithm.

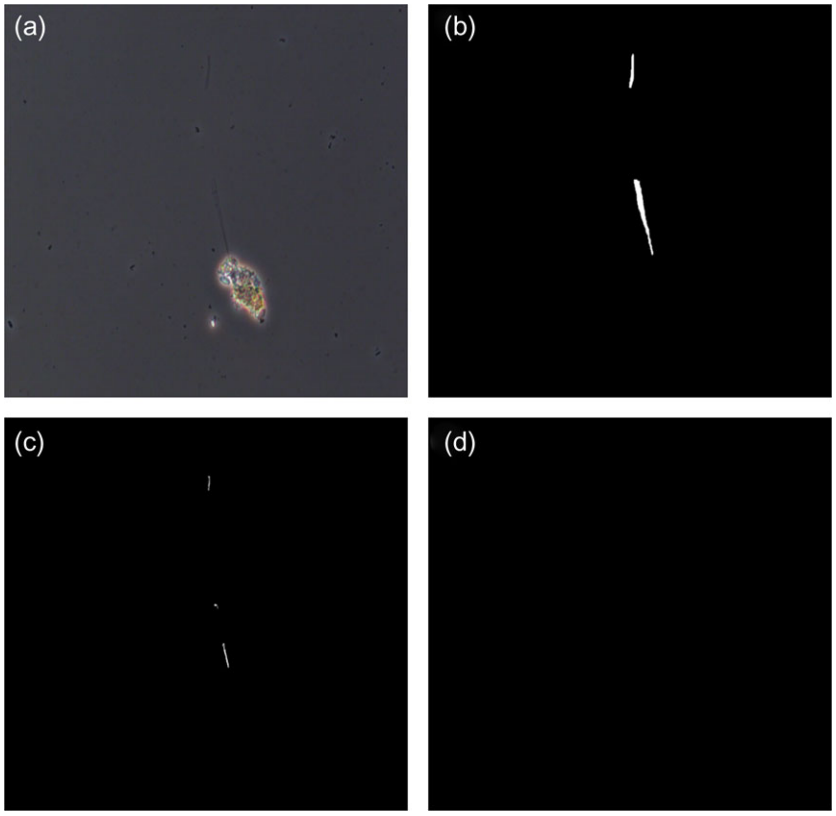

Fig. 13. Image and its segmentation with best FPR: (a) original image, (b) ground truth image, (c) proposed algorithm and (d) Sobel-based algorithm.

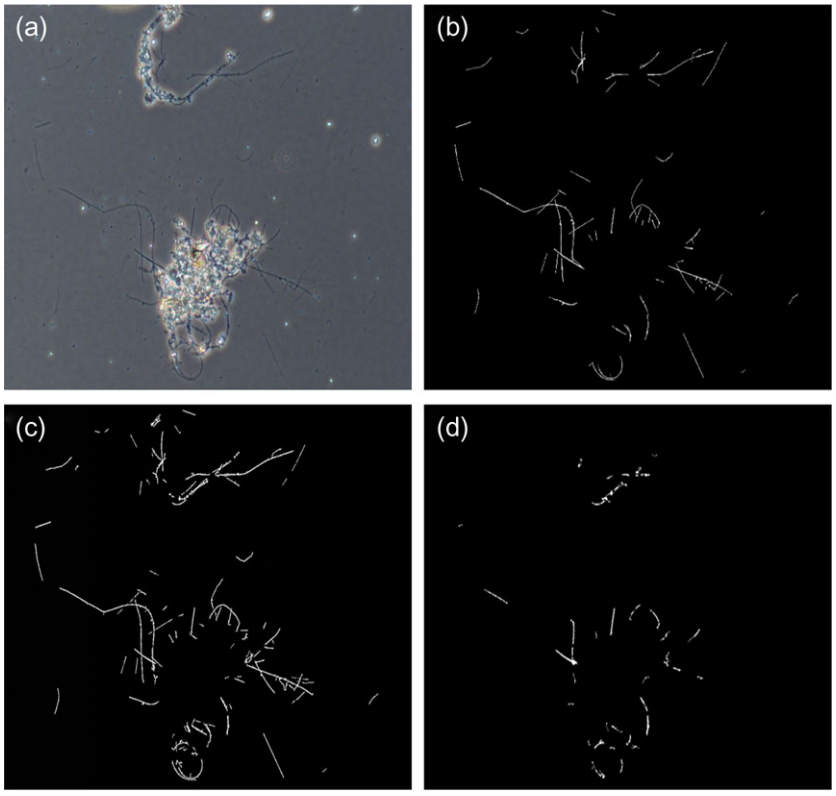

Fig. 14. Image and its segmentation with worst FPR: (a) original image, (b) ground truth image, (c) proposed algorithm and (d) Sobel-based algorithm.

segmented at 10× and 20× magnifications. The segmentation algorithm is based on PST. Phase kernel has been constructed by varying strength (S) and warp (W) values, empirically choosing $S = 0.4$ and $W = 40$ resulting in good segmentation accuracy decreasing the effect of shade-off artefact, however it increases foreground noise. Foreground noise is removed using specific methods during post-processing. In order to counter the halo artefact in phase contrast images negative phases have been removed by thresholding the phase image using a positive threshold equal to .002. The performance of the segmentation algorithm was assessed for different magnifications using DICE coefficient, accuracy, FNR, FPR and RI. The segmentation algorithm is more suitable at 10x magnification as it performed better with respect to the DICE coefficient and FNR with low variation. An average accuracy of 99.74%, RI of 99.49%, FNR of 41.8% and FPR of 0.14% have been achieved based on 61 images. The proposed filament segmentation algorithm shows better performance compared to the other algorithms reported in the literature in terms of accuracy, RI and FNR. The algorithm is invariant towards the halo artefacts of phase contrast images but sensitive towards the shade-off artefact. In the future, work can be extended to investigate post-processing methods to deal with 'false filaments' caused by shade-off artefacts. Effective floc and filament recognition techniques should be explored so that true filaments can be identified correctly, hence, increasing the accuracy of filament segmentation.

Acknowledgement

Figures 3a and 12a and b are obtained from Khan et al. [12] © Microscopy Society of America 2017, published by Cambridge University Press, reproduced with permission.

© [2018] IEEE. Reprinted, with permission, from Khan et al. [7].

References

1. Bitton G (2005) *Wastewater Microbiology*, (Hoboken, New Jersey: John Wiley & Sons).
2. Khan M B, Lee X Y, Nisar H, Ng C A, Yeap K H, Malik A S (2015). Digital image processing and analysis for activated sludge wastewater treatment. *Adv. Exp. Med. Biol.* 823, 227–248.
3. Mesquita D, Dias O, Amaral A, and Ferreira E (2010) A comparison between bright field and phase-contrast image analysis techniques in activated sludge morphological characterization. *Microsc. Microanal.* 16 (02): 166–174.
4. Khan M B, Nisar H, Ng C A, Lo P K, and Yap V V (2018) Generalized classification modeling of activated sludge process based on microscopic image analysis. *Environ. Technol.* 39 (1): 24–34.
5. Khan M B, Nisar H, Ng C A, and Lo P K (2016). Estimation of sludge volume index (SVI) using bright field activated sludge images. In: *2016 IEEE International Instrumentation and Measurement Technology Conference Proceedings (I2MTC)*, pp 1–5 (IEEE).
6. Mullins D, Coburn D, Hannon L, Jones E, Clifford E, and Glavin M (2018) Using image processing for determination of settled sludge volume. *Water Sci. Technol.* 78 (2): 390–401.
7. Khan M B, Nisar H, and Ng C A (2018) Image processing and analysis of phase-contrast microscopic images of activated sludge to monitor the wastewater treatment plants. *IEEE Access* 6: 1778–1791.
8. Kaur D, and Kaur Y (2014) Various image segmentation techniques: a review. *Int. J. Comput. Sci. Mobile Comput.* 3 (5): 809–814.
9. Lee X Y, Khan M B, Nisar H, Ho Y K, Ng C A, and Malik A S, 2014. Morphological analysis of activated sludge flocs and filaments. In: *2014 IEEE International Instrumentation and Measurement Technology Conference (I2MTC) Proceedings*, pp 1449–145. (IEEE).
10. Wu J, and Wheatley A (2010) Assessing activated sludge morphology by laser and image analysis. *Proc. Inst. Civ. Eng. Water Manag.* 163 (3): 139–145.
11. Nisar H, Hang H, Siang S, and Khan M. (2016). Image segmentation of microscopic wastewater images using phase contrast microscopy. In: *2016 IEEE Conference on Systems, Process and Control (ICSPC)*.
12. Khan M, Nisar H, Ng C, Yeap K, and Lai K (2017) Segmentation approach towards phase-contrast microscopic images of activated sludge to monitor the wastewater treatment. *Microsc. Microanal.* 23 (06): 1130–1142.
13. Jenné R, Cenens C, Geeraerd A, and Van Impe J (2002) Towards on-line quantification of flocs and filaments by image analysis. *Biotechnol. Lett.* 24 (11): 931–935.
14. Dias P, Dunkel T, Fajado D, Gallegos E, Denecke M, Wiedemann P, Schneider F, and Suhr H (2016) Image processing for identification and quantification of filamentous bacteria in in situ acquired images. *Biomed. Eng. Online* 15 (1): 64.
15. Asghari M, and Jalali B (2014). Physics-inspired image edge detection. In: *2014 IEEE Global Conference on Signal and Information Processing (GlobalSIP)*.
16. Asghari M, and Jalali B (2015) Edge detection in digital images using dispersive phase stretch transform. *Int. J. Biomed. Imaging* 2015: 1–6.
17. Suthar M, Asghari H, and Jalali B (2018) Feature enhancement in visually impaired images. *IEEE Access* 6: 1407–1415.
18. Suthar M, Mahjoubfar A, Seals K, Lee E W, and Jalaii B (2016). Diagnostic tool for pneumothorax. In: *2016 IEEE Photonics Society Summer Topical Meeting Series (SUM)*, pp 218–219 (IEEE).
19. Ilovitsh T, Jalali B, Asghari M H, and Zalevsky Z (2016) Phase stretch transform for super-resolution localization microscopy. *Biomed. Opt. Express* 7 (10): 4198–4209.
20. Jalali Lab *UCLA/Image-Feature-Detection-Using-Phase-Stretch-Transform*. [Online]. Available: https://github.com/JalaliLabUCLA/Image-feature-detection-using-Phase-Stretch-Transform/
21. Otsu N (1979) A threshold selection method from gray-level histograms. *IEEE Trans. Syst. Man Cybern.* 9 (1): 62–66.
22. Spencer Kimball, *Peter Mattis* (The GIMP Development Team) https://gitlab.gnome.org/GNOME/gimp.

23. Rand W (1971) Objective criteria for the evaluation of clustering methods. *J. Am. Stat. Assoc.* 66 (336): 846.
24. Lloyd S (1982) Least squares quantization in PCM. *IEEE Trans. Inf. Theory* 28: 129–137.
25. Meyer F (1994) Topographic distance and watershed lines. *Signal Processing* 38 (1): 113–125.
26. Kittler J, and Illingworth J (1986) Minimum error thresholding. *Pattern Recognit.* 19 (1): 41–47.
27. Jenné R, Banadda E N, Smets I, Deurinck J, and Van Impe J (2007) Detection of filamentous bulking problems: developing an image analysis system for sludge composition monitoring. *Microsc. Microanal.* 13 (1): 36–41.